

Stratospheric ozone in 3-D models: A simple chemistry and the cross-tropopause flux

C. A. McLinden, S. C. Olsen, B. Hannegan,¹ O. Wild,² and M. J. Prather

Department of Earth System Science, University of California at Irvine

J. Sundet

Department of Geophysics, University of Oslo, Oslo

Abstract. Two simple and computationally efficient models for simulating stratospheric ozone in three-dimensional global transport models are presented. The first, linearized ozone (or Linoz), is a first-order Taylor expansion of stratospheric chemical rates in which the ozone tendency has been linearized about the local ozone mixing ratio, temperature, and the overhead column ozone density. The second, synthetic ozone (or Synoz), is a passive, ozone-like tracer released into the stratosphere at a rate equivalent to that of the cross-tropopause ozone flux which, based on measurements and tracer-tracer correlations, we have calculated to be 475 ± 120 Tg/yr. Linoz and Synoz have been evaluated in the UC Irvine chemical transport model (CTM) with three different archived meteorological fields: the Goddard Institute for Space Studies (GISS) general circulation model (GCM) version II', the GISS GCM version II, and merged forecast data from the European Centre forecast model (EC/Oslo). Linoz produced realistic annual, cross-tropopause fluxes of 421 Tg/yr for the GISS II' winds and 458 Tg/yr for the EC/Oslo winds; the GISS II winds produced an unrealistic flux of 790 Tg/yr. Linoz and Synoz profiles in the vicinity of the tropopause using the GISS II' and EC/Oslo winds were found to be in good agreement with observations. We conclude that either approach may be adequate for a CTM focusing on tropospheric chemistry but that Linoz can also be used for calculating ozone fields interactively with the stratospheric circulation in a GCM. A future version of Linoz will allow for evolving background concentrations of key source gases, such as CH₄ and N₂O, and thus be applicable for long-term climate simulations.

1. Introduction

Since the 1950s, numerical models, which simulate the circulation of the atmosphere, have been used to gain insight into atmospheric phenomena and to make predictions on its future state [Phillips, 1956; Smagorinsky *et al.*, 1965]. Ever increasing computing power has allowed for three-dimensional (3-D) global chemical transport models (CTMs) and the inclusion of an ever greater number of chemical tracers controlled by even more detailed chemical mechanisms.

The current edge in tropospheric chemical transport modeling involves boundary layer and cloud coupling,

¹Now at Senate Energy and Natural Resources Committee, Washington, D.C.

²Now at Frontier Research System for Global Change, Tokyo.

Copyright 2000 by the American Geophysical Union.

Paper number 2000JD900124.
0148-0227/00/2000JD900124\$09.00

complex hydrocarbon chemistry, the combination of sulfur and aerosol chemistry with gas-phase chemistry, and the combination of tropospheric chemistry with climate modeling [e.g., Hauglustaine *et al.*, 1998; Wang *et al.*, 1998; Crutzen *et al.*, 1999; Wild *et al.*, 2000]. A key upper boundary condition, and long-standing problem, for these models is the stratosphere, which controls the flux of ozone into the troposphere as well as the ultraviolet radiation field driving the photochemistry. Concurrent development in global stratospheric chemistry models has progressed to 3-D models carrying 50+ species and being applied to the patchy, heterogeneous chemistry in the lower stratosphere that occurs on scales below most models' resolution [e.g., Douglass *et al.*, 1997; de Grandpré *et al.*, 1997; Steil *et al.*, 1998; Chipperfield, 1999; Rozanov *et al.*, 1999]. However, these models are not suitable for coupling with general circulation models (GCMs) for long-term climate simulations, and even their merging with tropospheric CTMs represents a major challenge. Thus we develop alternative models for stratospheric ozone that can be incorporated readily

in tropospheric CTMs or climate models. These simplified stratospheric ozone simulations are, of course, not intended to be competitive with the stratospheric CTMs in terms of chemical processes but, like their big cousins, are derived from current photochemical mechanisms, cross sections, and rate constants.

Our primary goals in developing a stratospheric ozone chemistry for atmospheric models that focus on the troposphere are (1) accurate calculation of the cross-tropopause flux, and (2) reasonable representation of the ozone gradients near the tropopause. Generally, in tropospheric CTMs, stratospheric ozone has been handled by specifying climatology-based mixing ratios for ozone in the lower stratosphere and then allowing the transport to determine the cross-tropopause flux [e.g., *Isaksen and Jackman, 1999*]. The stratospheric level at which the ozone mixing ratios are specified, as well as other factors affecting the flux, vary from model to model. The fluxes produced by recent models using variants of this technique range from over 1400 Tg/yr [*Crutzen et al., 1999*], to less than 400 Tg/yr [*Hauglustaine et al., 1998*]. Such discrepancies are important to resolve since they give almost opposite interpretations of the role of tropospheric photochemistry: the large fluxes result in net photochemical loss of ozone throughout most of the troposphere, whereas the much smaller fluxes require a net production in order to balance with near-surface losses.

We develop two simple and computationally efficient ozone models in this paper. The first is an interactive linear model for ozone (Linoz) chemistry. Such a model was first used in 3-D models by *Cariolle and Déqué [1986]* and later by *Prather et al. [1990]*. In this method the ozone chemical tendency is expressed as a linear function of ozone, temperature, and the overhead ozone column. The linearizations are performed about an observed climatological state for a standard set of latitudes, months, and altitudes. The 24-hour, zonal-mean ozone photochemical tendency is calculated at each time step for each stratospheric grid box from these monthly varying coefficients. The second method treats ozone as an inert tracer released in the stratosphere at a rate equivalent to that of the annual cross-tropopause ozone flux, a prescribed quantity. This is referred to as synthetic ozone (or Synoz). Linoz and Synoz require only a single tracer with negligible CPU requirements for the “chemistry”. Both allow the transport of ozone across the tropopause to be controlled by the model circulation, with the total annual flux fixed for Synoz but unconstrained for Linoz.

These ozone models are evaluated in the University of California at Irvine (UCI) CTM, an off-line, three-dimensional, global model driven by archived meteorological fields. Advection is carried out through conservation of second-order moments [*Prather, 1986*]. This CTM (and older versions) have been used in a number of studies [*Hall and Prather, 1995; Avallone and Prather, 1997; Hannegan et al., 1998; Wild et al., 2000*] and was

a participant in the “Models and Measurements 2” intercomparison [*Hall et al., 1999*]. In the present study the UCI CTM is driven with three sets of meteorological fields. The first two sets are archived output from the Goddard Institute for Space Studies (GISS) general circulation middle-atmosphere model version II' [*Koch and Rind, 1998*], denoted as GISS II', and the previous version, denoted as GISS II [*Rind et al., 1988*]. The third set is output from the European Centre forecast model in conjunction with the University of Oslo (EC/Oslo) [*Sundet, 1997*]. The GISS II' fields, originally at 4° latitude \times 5° longitude \times 31 layers ($4^\circ \times 5^\circ \times 31$), have been degraded to $8^\circ \times 10^\circ \times 23$. This degradation was found to have only a minor impact on results. The GISS II fields, originally at $7.8^\circ \times 10^\circ \times 23$, are run at $7.8^\circ \times 10^\circ \times 21$. In both cases the uppermost layers of the GCM are concatenated into a single CTM layer. In the GISS II simulations, horizontal diffusion between levels 4 and 7 (~ 900 – 300 hPa) has been added to allow for increased interhemispheric transport and tropospheric mixing [*Prather et al., 1987*]. The EC/Oslo fields are generated at T63 but are used at T21 (about $5.6^\circ \times 5.6^\circ$) and have 19 layers with a ceiling at 2 hPa. The vertical coordinates of all three fields are shown in Figure 1.

In addition to its use in tropospheric models, Linoz is also well suited for use in GCMs where it can be run interactively through coupling to on-line heating rates. Future applications envisioned for Linoz include linking to long-lived source gases such as CH_4 and N_2O for 21st century climate change studies.

The remainder of this paper is organized as follows: Linoz is presented in section 2, including its formula-

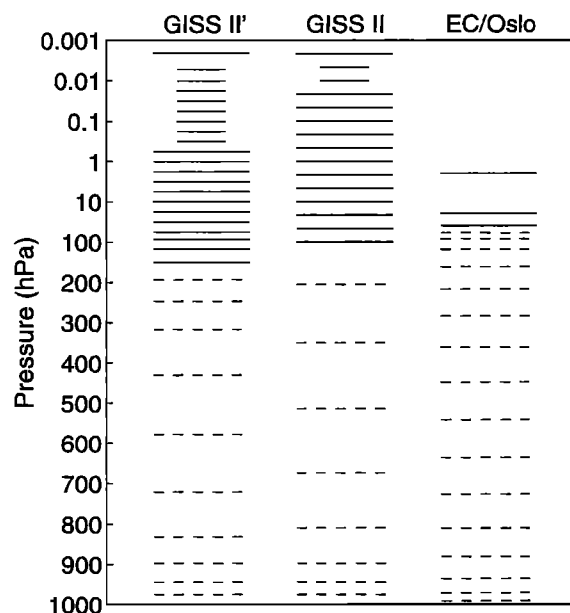


Figure 1. Model level edges of the GISS II', GISS II, and EC/Oslo meteorological fields. Dashed lines indicate hybrid levels (using a surface pressure of 1000 hPa), and solid lines are constant pressure levels. Shorter solid lines indicate additional levels used by the GISS GCM but grouped together in CTM simulations.

tion, climatologies, and cross-tropopause flux. Likewise, Synoz is presented in section 3. A summary of key conclusions and future directions is given in section 4.

2. Linearized Ozone (Linoz)

2.1. Linoz Formulation

Cariolle and Déqué [1986] were the first to include a linearized ozone scheme in a three-dimensional model. We follow their basic parameterization and expand the ozone tendency to first order about the local ozone mixing ratio, temperature, and overhead column ozone. In the following, it is assumed that key families (NO_y , Cl_y , Br_y) and long-lived gases (N_2O , CH_4 , H_2O) experience low variability and that their small-scale fluctuations would not produce ozone tendencies significantly different from the use of a mean distribution. Under these conditions, deviations of the ozone tendency from its climatological value can be calculated in terms of these three quantities. The change in ozone with time due to local chemistry is given by,

$$\frac{df}{dt} = (P - L)[f, T, c_{\text{O}_3}], \quad (1)$$

where $(P - L)$ represents the ozone tendency (in units of ppmv/s), the square brackets denote a functional dependence, f is the ozone mixing ratio, T is temperature, and c_{O_3} is the column ozone above the point under consideration. Equation (1) is expanded to first order in a Taylor series,

$$\begin{aligned} \frac{df}{dt} = & (P - L)^{\circ} + \left. \frac{\partial(P - L)}{\partial f} \right|_{\circ} (f - f^{\circ}) + \\ & \left. \frac{\partial(P - L)}{\partial T} \right|_{\circ} (T - T^{\circ}) + \left. \frac{\partial(P - L)}{\partial c_{\text{O}_3}} \right|_{\circ} (c - c_{\text{O}_3}^{\circ}), \end{aligned} \quad (2)$$

where the superscript "o" represents climatological values and subscript "o" denotes evaluation of the partial derivatives at f° , T° , and $c_{\text{O}_3}^{\circ}$. The climatologies for ozone (and column ozone) [*McPeters*, 1993] and tem-

perature [*Nagatani and Rosenfield*, 1993] are adopted from the "Models and Measurements 1" intercomparison (hereinafter referred to as the observed climatology).

By defining a time constant τ and a steady state mixing ratio (in the absence of dynamics) f^{ss} ,

$$\tau \equiv - \left[\left. \frac{\partial(P - L)}{\partial f} \right|_{\circ} \right]^{-1}, \quad (3)$$

$$\begin{aligned} f^{ss} \equiv & f^{\circ} + \left[(P - L)^{\circ} + \left. \frac{\partial(P - L)}{\partial T} \right|_{\circ} (T - T^{\circ}) + \right. \\ & \left. \left. \frac{\partial(P - L)}{\partial c_{\text{O}_3}} \right|_{\circ} (c_{\text{O}_3} - c_{\text{O}_3}^{\circ}) \right] \tau, \end{aligned} \quad (4)$$

equation (3) can be rewritten in the more compact form

$$\frac{df}{dt} = \frac{(f^{ss} - f)}{\tau}. \quad (5)$$

Assuming τ and f^{ss} remain constant over the model time step t to $t + \Delta t$, equation (5) can be integrated analytically to

$$f^{t+\Delta t} = f^t + (f^{ss} - f^t)(1 - e^{-\Delta t/\tau}). \quad (6)$$

The analytic solution has the advantage of allowing a stable limit for model time steps larger than the time constant.

The time constant τ defines the photochemical relaxation time (as a linearization of the loss) and is shown in Figure 2 for January and April. A rapid increase from an hour or so in the upper stratosphere to several months or years in the lower stratosphere is observed. A maximum (i.e., infinity) occurs during the polar night and also in the lowest few kilometers of the tropical stratosphere where production via O_2 photolysis greatly exceeds loss and drives the rate of change of ozone. In the middle to upper stratosphere, because chemical timescales are short, ozone is very close to steady state; however, this steady state mixing ratio (f^{ss}) is not necessarily equal to the observed climatological value (f°). Our linearized model calculates the

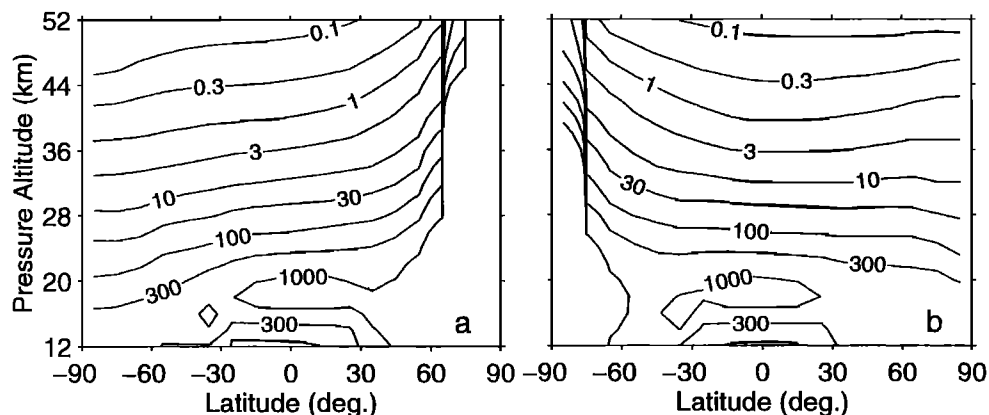


Figure 2. Photochemical relaxation time (in days), defined by linearization of the loss, as a function of latitude and pressure altitude for (a) January and (b) April.

same ozone that most full chemistry models would and underpredicts ozone in the upper stratosphere. Linoz does not solve this long-standing photochemical problem.

In the lower stratosphere where ozone is far from steady state, $(P-L)^o > 0$ in the tropics and $(P-L)^o < 0$ in the extratropics. The Brewer-Dobson circulation transports air from the tropical source region to the midlatitudes and polar regions: $f^{ss} > f^o$ in the tropics and $f^{ss} < f^o$ in the extratropics. Note that since f^{ss} is a linear extrapolation from the observed climatological, it may imply a negative steady state mixing ratio. This is neither a logical nor a practical problem. In reality, our assumed linearization breaks down as f is substantially decreased; and in practicality, the chemical timescale is much longer than that for transport, so negative mixing ratios are never actually reached.

Ozone chemistry is inherently nonlinear, and the validity of our first-order approximation can be assessed by examining the degree of nonlinearity experienced by the tendency. Figure 3 compares the exact and Linoz tendencies as a function of local ozone, temperature, and column ozone at four pressure altitudes ($z^* = 16, 24, 32,$ and 40 km where $z^* = 16 \log_{10}(1000/P)$ is pressure altitude (km) and P is pressure (hPa)), for May at 45°N . The ranges chosen for each represents a reasonable upper end of natural variability (excluding large polar ozone depletion) about the observed climatology: local ozone, $\pm 50\%$, temperature, ± 20 K, and

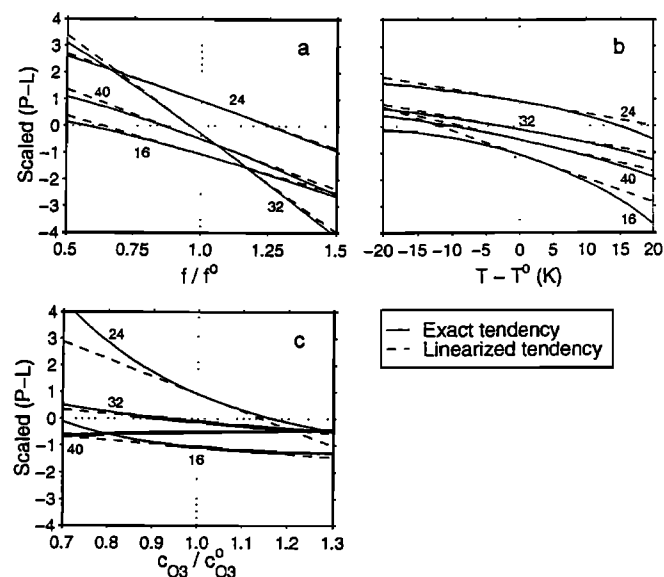


Figure 3. Comparison of exact (solid) and linearized (dashed) ozone tendencies for May, 45°N , at selected pressure altitudes (km), as indicated, as a function of (a) local ozone, (b) temperature, and (c) column ozone. Tendencies have been scaled and can be converted to real units through multiplication of the ordinates by $2.5 \times 10^6 \text{ cm}^{-3} \text{ s}^{-1}$ at 40 km, $1.25 \times 10^6 \text{ cm}^{-3} \text{ s}^{-1}$ at 32 km, $1.25 \times 10^5 \text{ cm}^{-3} \text{ s}^{-1}$ at 24 km, and $2.5 \times 10^4 \text{ cm}^{-3} \text{ s}^{-1}$ at 16 km.

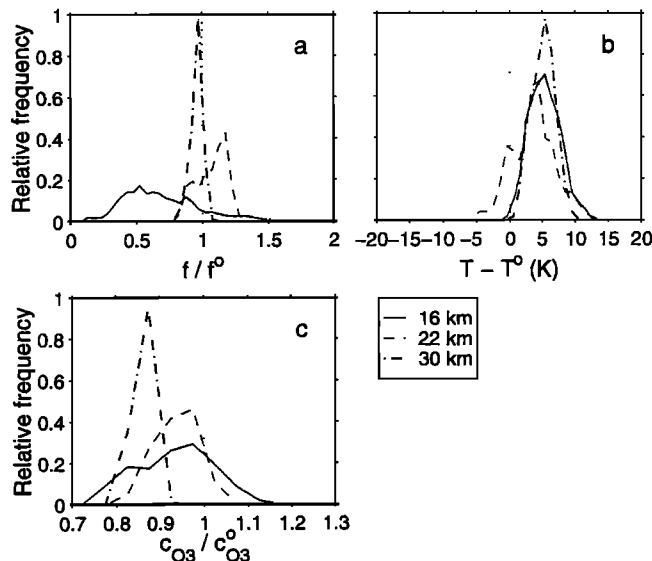


Figure 4. Monthly probability distribution (or relative frequency) from the GISS II' model for (a) local ozone, (b) temperature, and (c) column ozone for May around the 45°N latitude circle at three pressure altitudes: 16 km (solid), 22 km (dashed), and 30 km (dotted-dashed). The abscissa has been scaled (ozone and column ozone) or shifted (temperature) to the observed climatology (a value of 1 for ozone and column ozone and zero for temperature), and demonstrates, for example, the systematically high temperatures of the GISS II' meteorology. Each distribution is based on 4464 points (31 days, 4 times steps per day, and 36 longitudes).

column ozone, $\pm 30\%$. There are no significant differences between exact and linearized tendencies over a reasonable range of local ozone mixing ratios, even at half the climatological value. Tendency variation as a function of temperature and column ozone experience larger nonlinearities: temperature at $+20$ K overestimates the tendency by up to 20% and column ozone at -30% underestimates it by up to 30% in the lower stratosphere. Nonetheless, even these worst cases remain reasonable, and further, their impact is mitigated somewhat as they occur in the lower stratosphere, where chemistry is relatively slow. The overall linearity for May, 45°N , is representative of other months and latitudes.

Using results from a GISS II' simulation (details described below), the distribution of local ozone, temperature, and column ozone about the observed climatology can be examined to verify that the majority of values fall within this linear regime. At three CTM levels ($z^* = 16, 22,$ and 30 km), all values of ozone, temperature, and column at 45°N in May have been plotted as a probability distribution in Figure 4. Only the local ozone at 16 km has a significant fraction (1278 of 4464 points) of its distribution outside the range defined above, although even here the assumption of linearity remains reasonable to $0.3f^o$. These results are fairly typical: distributions are widest in the lower strato-

sphere where the tail of the local ozone distribution is beyond $\pm 50\%$.

Linoz consists of seven sets of tabulated coefficients (we make the distinction from look-up tables which require on-line interpolation) calculated at 25 pressure altitudes from $z^* = 10$ to 58 km at 2 km increments, 18 latitudes (-85°S , -75°S , ..., 85°N), and 12 months. The first four sets of coefficients give the diurnally averaged climatological ozone tendency and the three partial derivatives from equation (3) calculated using the photochemical box model of Prather [1992] and Prather and Jaffe [1990] (details given in Appendix). Note that in the tropics around 16 km there is a net photochemical ozone production due to O_2 photolysis of about 1 ppbv/d. The remaining three sets contain the ozone and column ozone climatologies [McPeters, 1993] and the temperature climatologies [Nagatani and Rosenfeld, 1993]. Use of other similar climatologies should not significantly affect the simulations. The linearization terms (i.e., the partial derivatives) are determined by perturbing the local ozone, temperature, and column ozone separately and recalculating radicals and the diurnally averaged tendency. The perturbations were +5% in local ozone, +4 K in temperature, and +5% in column ozone. Note that the column perturbation is treated as a purely radiative change (i.e., photolysis rates) in order to isolate its effects from the local ozone perturbation. Further details concerning the photochemical calculations are given in the Appendix.

Linoz is implemented in any CTM by a once-per-month remapping of the coefficients onto the CTM latitude and altitude grids effectively generating the set of seven tables specific to the model grid. This is done through linear interpolation in latitude and by averaging the coefficients, originally calculated at 2-km increments in pressure altitude, over the CTM layers. In operation the chemically driven change in ozone in a grid box is determined directly from equation (6) evaluated at the midpoint of each grid box. The value of local ozone is simply the mean over a grid box (or the zeroth order moment) while temperature is obtained from the archived meteorological fields. The total column above a layer is calculated by integrating over the layers above and includes half of the column in the layer under consideration.

Note that the chemistry is directly coupled only to the mean, or zeroth order moment, so any change in ozone due to chemistry is evenly distributed throughout the model grid box. Upon completion of the chemistry, the first- and second-order moments are then scaled by the chemistry-induced fractional change in ozone mass.

2.2. Linoz Climatology

In this section we examine the Linoz climatologies derived using the GISS II', GISS II, and EC/Oslo meteorologies and compare them with the observed climatology. Each is taken as the final year of a 5-year integration initialized with the observed climatology. In

each case, the single year of winds is recycled, and thus interannual variability is not simulated. Tropospheric ozone production and surface deposition is simulated by relaxing ozone in the lowest three model levels to 25 ppbv with a 2-day e -fold. Note that in the upper stratosphere, ozone relaxes to the steady state derived from the chemical model and not the observed steady state as was done by Prather *et al.* [1990].

The GISS II' annual, zonal-mean Linoz tendency is shown in Figure 5. Above $z^* = 35$ km or so, the production and loss is balanced. Below this in the equatorial region there is excess production which peaks near the ozone maximum. The midlatitudes show an approximate balance, while excess loss occurs in the polar regions. This is consistent with models running full stratospheric chemistry [de Grandpré *et al.*, 1997].

The Linoz Dobson maps (or zonal, monthly-mean ozone column densities) are presented in Figure 6 along with the observed climatology. In the calculation of the EC/Oslo maps it was necessary to add the climatological ozone column above the model top at 2 hPa, about 5–8 Dobson Units (DU). The EC/Oslo climatology (Figure 6b) is in excellent agreement with the observed climatology (Figure 6a) despite having only one level between 20 and 2 hPa ($z^* = 27 - 43$ km; see Figure 1). This agreement includes the Southern and Northern Hemisphere maximums and the midlatitude gradients. An ozone hole is not simulated due to the lack of polar stratospheric cloud (PSC) chemistry in Linoz. The tropics are also generally consistent with observations, but some anomalous structure appears (e.g., a local maximum of about 310 DU centered on the equator in August). This is probably the result of inappropriate averaging of the Linoz coefficients over the EC/Oslo 20–2 hPa level which may contain up to 120 DU in the tropics, or roughly half the stratospheric column. The GISS II map (Figure 6c), which does not include temperature feedback because temperature was not recorded in the meteorological fields, displays the same basic structure as the observed climatology but is deficient in several ways. The tropical minimum is roughly 20 DU below the observations, and the latitudinal gradients though the midlatitude autumns are too steep. The magnitude of the Northern and Southern Hemisphere peaks agree with observations, but the Southern Hemisphere peak spans 40° in latitude and persists for four months.

GISS II' Linoz climatologies are shown for the local ozone feedback only (Figure 6d), local and column ozone feedback (Figure 6e) and local ozone, temperature, and column ozone feedback (Figure 6f). All three are similar and agree with the observed climatology quite well in seasonal and latitudinal trends as well as absolute values. The exception to this is the Southern Hemisphere winter and spring south of 40° . The Southern Hemisphere maximum is not offset from the pole as expected but peaks at the pole and is roughly 60 DU too large (100 DU when including temperature feedback).

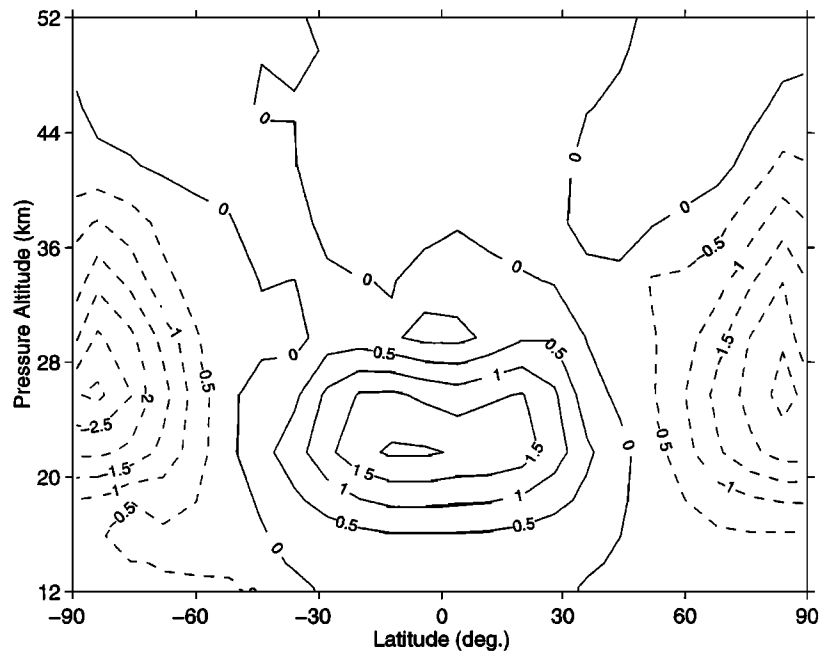


Figure 5. GISS II' annual, zonal-mean Linoz tendency (or residual production) in units of 10^5 molecules $\text{cm}^{-3} \text{s}^{-1}$. (Linoz does not include “ozone hole”/PSC-type chemistry.)

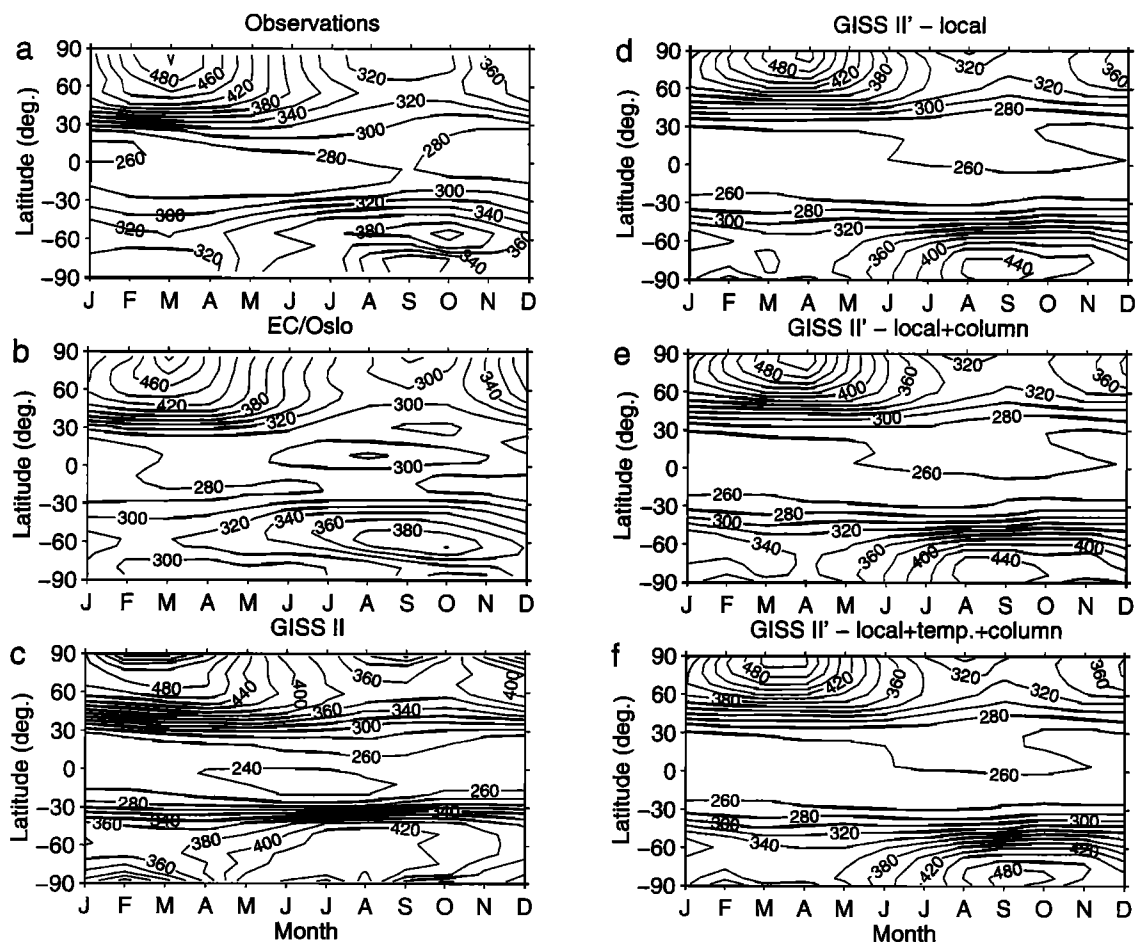


Figure 6. Zonal, monthly-mean column ozone density in Dobson Units (DU) for (a) observed climatology and for various Linoz climatologies: (b) EC/Oslo (including local ozone, temperature, and column feedbacks), (c) GISS II (local and column ozone feedbacks), (d) GISS II' (local ozone feedback only), (e) GISS II' (local and column ozone feedback), and (f) GISS II' (local ozone, temperature, and column feedbacks). “Ozone hole”/PSC-type chemistry is not included in Linoz.

This feature (also observed in the GISS II map) is dynamic in origin and is discussed further in section 2.3. The addition of the column ozone feedback term acts to slightly increase the column values in the midlatitude and polar regions by roughly 5–10 DU due to an approximate 10% underestimate of ozone through the middle and upper stratosphere, as shown below. The zonal, monthly-mean GISS II' temperatures are generally 0–15 K warmer than climatology (compare with Figure 4b) which leads to a decrease in ozone. Exceptions to this are mainly in the lower stratosphere where the bulk of the column resides; cooler temperatures lead to an increase in ozone (and hence ozone column), particularly in the polar regions.

Zonal, monthly-mean profiles for January are shown in Figure 7. Overall, the Linoz climatologies were in excellent agreement with observations; the shape and seasonality of the profiles were captured, while their magnitude was in good overall agreement displaying, 10–20% errors. All climatologies (except the EC/Oslo which extends only to $z^* = 30$ km) systematically underestimates the ozone in the upper stratosphere by 10–20% as compared with our adopted climatology. Note that Linoz drives the model toward the photochemical balance, not toward the climatology. This “ozone deficit” is common to all photochemical models adopt-

ing “current” chemistry (i.e., the rates from *DeMore et al.* [1997]) and the extent to which this persistent discrepancy is real (e.g., missing chemistry) or simply a problem with photochemical rates remains uncertain [WMO, 1999]. Another common characteristic of the Linoz climatologies is the underestimate of the ozone maximum in the tropics near 35 km by roughly 0.5–1 ppmv, a difference which increases when the column feedback is not included as observed in the GISS II' simulations. Thus inclusion of the column feedback term acts to push ozone back toward the observed climatology and illustrates the so-called ozone “self-healing” effect [e.g., *Brasseur and Solomon*, 1986]. The effects of the generally warmer than climatology temperatures in the GISS II' fields are clearer in the profiles: a decrease in ozone through the middle and upper stratosphere as is evident from the reduced maximums and the pinched-off 5 ppmv contour at the South Pole (as compared with the local and column feedback climatologies).

Finally, the stability of Linoz has been tested by initializing, using 0.2 and 5 times the observed climatology with the GISS II' meteorological fields. In these cases, ozone rapidly converged back to the same steady state shown in Figures 6 and 7. Its stability and performance when run interactively in a GCM has not yet been assessed; however, testing in the GISS GCM is under way.

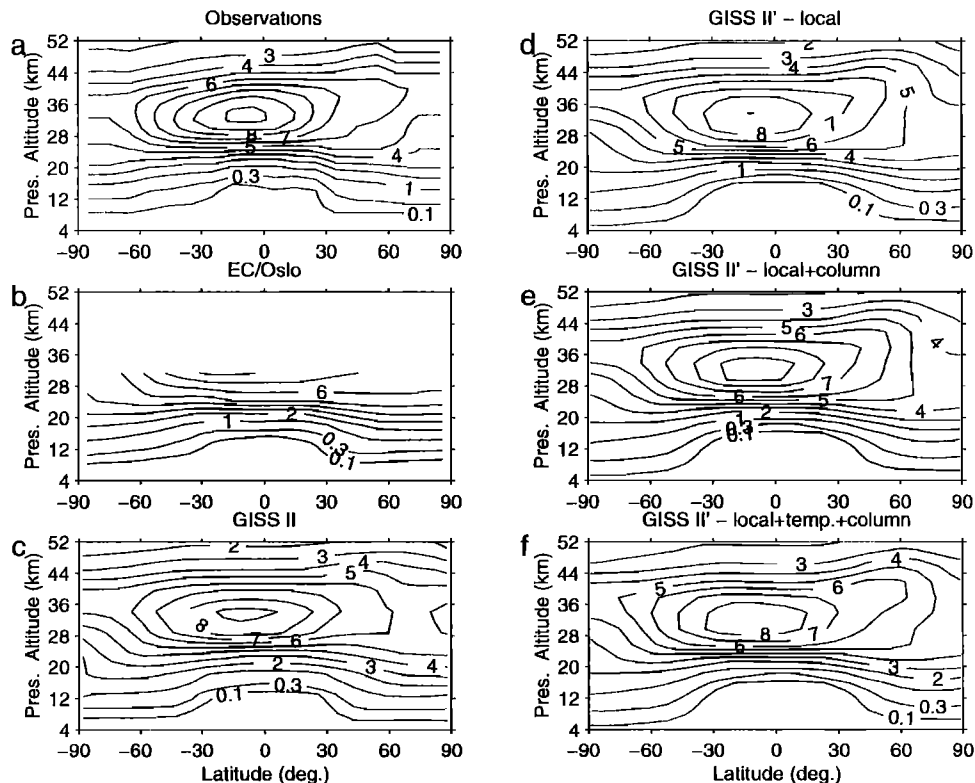


Figure 7. January zonal-mean ozone mixing ratio (ppmv) for (a) observed climatology, and for various Linoz climatologies: (b) EC/Oslo (including local ozone, temperature, and column feedbacks), (c) GISS II (local and column ozone feedbacks), (d) GISS II' (local ozone feedback only), (e) GISS II' (local and column ozone feedback), and (f) GISS II' (local ozone, temperature, and column feedbacks). “Ozone hole”/PSC-type chemistry is not included in Linoz.

Table 1. Linearized and Synthetic Ozone Annual Budgets and Cross-Tropopause Fluxes

	Linearized Ozone			Synthetic Ozone		
	GISS II'	EC/Oslo	GISS II	GISS II'	EC/Oslo	GISS II
	<i>Stratosphere</i>					
Burden (Tg) ^a	2934	3127 ^b	3145	–	–	–
Net Production (Tg/yr)	421	458	790	–	–	–
Release Rate (Tg/yr)	–	–	–	475	475	475
	<i>Cross-Tropopause Flux</i>					
Total (Tg/yr)	421	458	790	475	475	475
N-S Ratio	0.89	1.61	1.09	0.90	1.41	1.00
% > 60°N	21	0	3	18	0	2
% > 60°S	23	–3 ^c	16	20	–2 ^c	14
	<i>Troposphere</i>					
Burden (Tg) ^a	250	251	259	227	241	197

The tropopause is defined at 300 hPa from 90°S to 30°S, 100 hPa between 30°S and 30°N, and 300 hPa from 30°N to 90°N.

^aOn January 1.

^bIncludes climatology above 2 hPa.

^cNet transport into stratosphere.

2.3. Cross-Tropopause Ozone Flux

Table 1 summarizes the Linoz annual budgets and cross-tropopause fluxes. These calculations are based on an approximate tropopause, which is defined at 300 hPa from 90°S to 30°S, 100 hPa between 30°S and 30°N, and 300 hPa from 30°N to 90°N. The global, annual cross-tropopause fluxes are 421 Tg (GISS II'), 458 Tg (EC/Oslo), and 790 Tg (GISS II). The GISS II' and EC/Oslo fluxes compare well with our best estimate of 475 ± 120 Tg based on measurements and tracer-tracer correlations (discussed below), while the GISS II flux is unrealistically large. For each calculation the annual cross-tropopause flux was equivalent to the net annual stratospheric production and the net annual tropospheric destruction. Unfortunately, studies of the cross-tropopause flux of air mass [e.g., Appenzeller *et al.*, 1996] are not readily scaled to the ozone flux without a complete reanalysis. The GISS II' and GISS II fluxes show only a small hemispheric asymmetry, while the EC/Oslo has two thirds of its net flux occurring in the Northern Hemisphere. The tropospheric burdens, though clearly underestimating ozone production in the free troposphere compare with models running tropospheric chemistry [e.g., Haughustaine *et al.*, 1999], are reasonable.

In the GISS II' simulation, a large fraction of the cross-tropopause transport occurs at the poles (also the case at the South Pole in the GISS II simulation). This is not seen in the EC/Oslo simulation (based on forecasts from analyzed fields) and, further, is inconsistent with our current understanding of stratosphere-troposphere exchange [WMO, 1999].

This discrepancy is clearly seen when the ozone mixing ratio is used as a diagnostic of the tracer tropopause, as in Figure 8. Typically, the transition from troposphere to stratosphere occurs at about 100 ppbv of ozone [Logan, 1999a], and Figure 8 shows the pressure

altitude of the 100 and 200 ppbv contours for the GISS II' and EC/Oslo climatologies in January, each compared to observations.

The GISS II' contours are at lower altitudes, relative to observation, by up to 4 km at the South Pole and 2 km in the North Pole. In the tropics the opposite is true: the GISS II' contours are up to 2 km higher than observations, which may indicate a high tropical tropopause. The EC/Oslo contours compare much better with the climatology, generally within 1 km. Linoz profiles are evaluated through comparisons with monthly averages of multiyear ozonesonde data [Logan, 1999a, b]. GISS II', EC/Oslo, and sonde profiles for the midtroposphere to lower stratosphere July means are shown in Figure 9 at six stations: Alert, Edmonton, Hohenpeissenberg, Hilo, Natal, and Lauder. Note that zonal means are no longer used and that a linear scale is employed to emphasize the tropopause and lower stratosphere. Clearly, there is good agreement between the Linoz and the sonde profiles at all stations with little to choose from between the GISS II' and the EC/Oslo profiles. Note that these plots may mask differences of up to 30 ppbv in the troposphere.

3. Synthetic Ozone (Synoz)

3.1. Definition

Synthetic ozone (Synoz) is a passive, ozone-like tracer released into the stratosphere at a rate equivalent to that of the prescribed cross-tropopause ozone flux. The release region is bounded by 30°S to 30°N and 70 to 10 hPa, so it mimics that in which chemistry predicts net photochemical production of ozone (see Figure 5). Inside this region, the release rate is constant in mixing ratio. As with Linoz, Synoz is relaxed to 25 ppbv with an e -fold of 2 days in the lower troposphere. In the absence of chemistry and in steady state, the global,

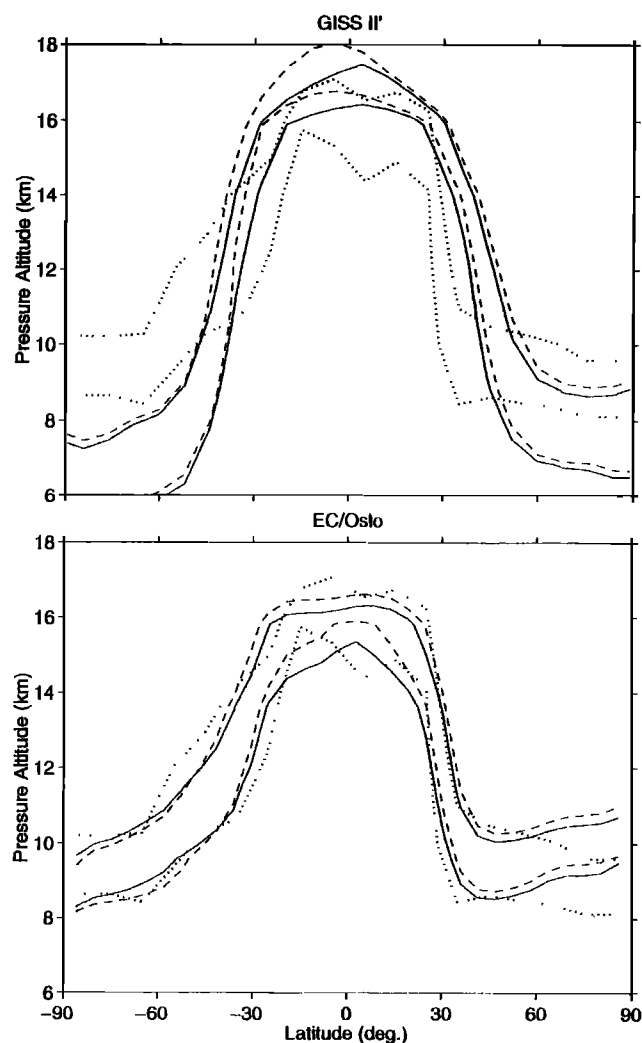


Figure 8. Diagnostic of tropopause, specifically the pressure altitude of the 100 and 200 ppbv zonal-mean ozone mixing ratio contours. Shown are Linoz (solid) and Synoz (dashed) for the GISS II' (top) and EC/Oslo fields (bottom) for January. These are compared with the observed climatology (dotted). The top curves in each panel represent the 200 ppbv contour.

annual cross-tropopause Synoz flux is thus forced to be identical to the total released into the stratosphere.

This technique ensures that the cross-tropopause flux of ozone can be matched to observational constraints and that it is controlled in terms of seasonality and location by the model circulation. In analogy with Linoz an ozone tropopause may be diagnosed based on a Synoz isopleth. Further, the separation of stratospheric and tropospheric air can be defined dynamically in the model on a grid box by grid box basis by the Synoz concentration. For example, in some UCI CTM applications the transition from stratospheric to tropospheric chemistry is defined as the Synoz 100 ppbv isopleth [Wild *et al.*, 2000]. Synoz may, in fact, be preferable to Linoz in models that have a coarsely resolved stratosphere or an unrealistic cross-tropopause flux (as was the case for the GISS II Linoz simulation).

3.2. Observed Cross-Tropopause Ozone Flux

This method requires an observational constraint for the global, annual cross-tropopause ozone flux a priori. The approach of *Murphy and Fahey* [1994] uses the observed N_2O - O_3 correlation to derive a cross-tropopause ozone flux by scaling to the reverse (upward) N_2O flux derived from models and measurements. Their value of $3.5 \times 10^{10} \text{ cm}^{-2} \text{ s}^{-1}$ is consistent with earlier estimates based on independent methods but is reported with large uncertainty. A problem with this derivation is the use of the N_2O - O_3 correlation: in the region of interest (50–500 ppbv of O_3), N_2O only varies by 10% (280–310 ppbv), making the correlation slope a poorly determined quantity. In addition, the N_2O flux into the stratosphere occurs mainly in the tropics, whereas the ozone return flux occurs primarily at midlatitudes. Observations reveal that these two regions have distinctly different correlation slopes. Thus the issue of which N_2O - O_3 relationship to use remains unclear.

We adopt a two-part transfer standard which we believe more accurately defines the ozone flux. The N_2O - NO_y and NO_y - O_3 correlations have tighter relationships, a smaller seasonality, and are more accurately determined with respect to instrument noise, than the N_2O - O_3 correlation. On the basis of a mean lifetime of $120(\pm 17\%) \text{ yr}$ [Ko *et al.*, 1991; IPCC, 1995] and a tropospheric mixing ratio of 310 ppbv, the flux of N_2O into the stratosphere is $1.67 \times 10^9(\pm 17\%) \text{ cm}^{-2} \text{ s}^{-1}$. The net yield of NO_y from N_2O is well defined from midlatitude measurements which are consistent with models and $\Delta NO_y/\Delta N_2O = -0.073(\pm 14\%)$ is the slope of the correlation [Keim *et al.*, 1997]. The NO_y/O_3 ratio observed at midlatitudes is $0.0033(\pm 12\%)$ with most data points falling within the range 0.0025 to 0.0040 [Murphy *et al.*, 1993; Fahey *et al.*, 1996]. These ratios are notably different in polar and tropical regions, but the total flux of these two downward moving tracers into the troposphere is dominated by the midlatitudes. Multiplying these three numbers gives an estimate of the cross-tropopause ozone flux: $3.7 \times 10^{10}(\pm 25\%) \text{ cm}^{-2} \text{ s}^{-1}$ or $475 \pm 120 \text{ Tg/yr}$.

The N_2O - NO_y correlation includes the effects of NO_y transported into the stratosphere across the tropical tropopause [Murphy and Fahey, 1994]. Also, the importance of denitrified stratospheric air entering the troposphere is expected to be small given that the poles represent a very small region of the globe. In addition, extensive measurements show that the correlation slope varies by less than 10% over a large range of latitudes and over all seasons [Murphy and Fahey, 1994], which means the impact of denitrification on the bulk stratosphere must also be included.

3.3. Synoz in the UCI CTM

On the basis of an ozone release rate of 475 Tg/yr in the stratosphere, the CTM was again run to steady state using the three sets of meteorological fields. The Synoz annual budgets and cross-tropopause fluxes are

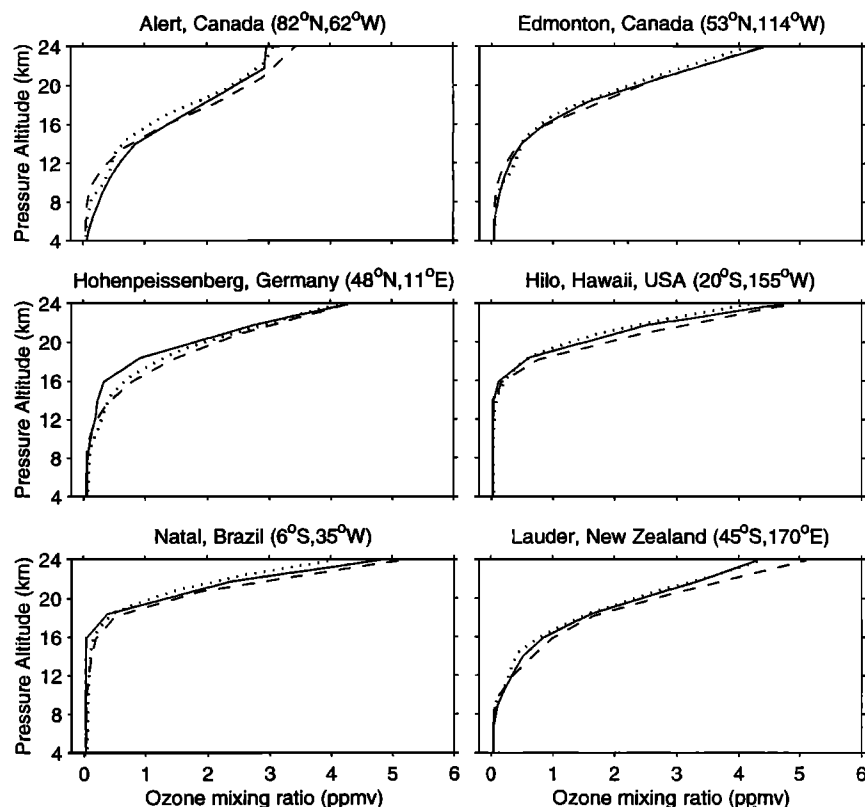


Figure 9. July ozone profiles at selected ozonesonde stations: GISS II' Linoz model (solid), EC/Oslo Linoz model (dashed), and multi year, monthly averaged ozonesonde data (dotted). A linear scale is used to emphasize the lower stratosphere (discrepancies in troposphere can be as large as 30 ppbv). Ozonesonde means based on 20 July soundings at Alert from 1988 to 1993, 46 July soundings at Edmonton from 1980 to 1993, 109 at Hohenpeissenberg from 1980 to 1993, 26 at Hilo from 1986 to 1993, 19 at Natal from 1978 to 1992, and 17 at Lauder from 1986 to 1990 [Logan, 1999a, b].

given in Table 1. The north-to-south ratio is similar to the Linoz simulation, and the polar problems with the GISS fields are still present. The Synoz tropospheric burdens are 10–60 Tg smaller than their Linoz counterparts due primarily to a lack of production in the tropical upper troposphere where Linoz includes O_2 photolysis (from Figure 5, about 1 ppbv/d).

The January 100 and 200 ppbv Synoz isopleths are compared with the corresponding Linoz and observed climatology isopleths in Figure 8. Overall, the shape of the Synoz contours closely resembles that of the Linoz contours are differences in contour heights are less than 1 km. The differences between the Synoz and Linoz contours are explained by the Synoz (1) lack of production in the tropical upper troposphere, (2) lack of destruction in the summer hemisphere extratropical stratosphere, and (3) static release region that is not shifted in latitude toward the summer hemisphere. The comparison of contour heights at other months was essentially identical, which further underscores the basic similarities between Synoz and observed ozone, a result not unexpected based on the slow photochemical evolution of ozone in the lowermost stratosphere. Of course, Synoz profiles above the lowermost stratosphere rapidly

diverge from observations and cannot be used to derive stratospheric ozone columns.

4. Summary

We present two simple and computationally efficient stratospheric ozone models for use in global atmospheric models. The first, linearized ozone (Linoz), is based on a first-order Taylor expansion of ozone tendency about local ozone mixing ratio, temperature, and overhead column ozone density. Using the UC Irvine chemical transport model (CTM) driven by GISS II', GISS II, and EC/Oslo meteorological fields, resultant linearized ozone climatologies were found to be in very good agreement with observations. The one notable exception is the GISS fields at the poles. The second, synthetic ozone (Synoz), is a passive, ozone-like tracer released into the stratosphere at a rate equivalent to that of the cross-tropopause ozone mass flux, which based on measured NO_y-N_2O and NO_y-O_3 correlations, we estimate to be 475 ± 120 Tg/yr.

Linoz produced a cross-tropopause ozone fluxes of 421 Tg/yr for the GISS II' winds and 458 Tg/yr for the EC/Oslo winds, consistent with our estimate of

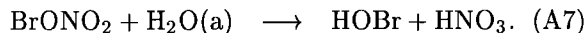
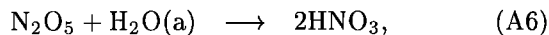
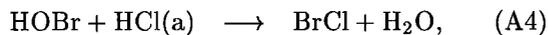
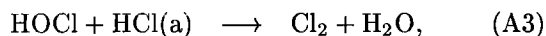
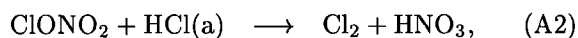
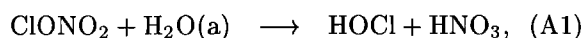
475 ± 120 Tg/yr. The height of both the Linoz and the Synoz 100 and 200 ppbv contours are in good agreement with observations when driven by the EC/Oslo fields; the GISS II' contours are also consistent with observations except in the polar regions.

These simulations indicate that either Linoz or Synoz are suitable candidates for an efficient and simple stratospheric ozone in tropospheric CTMs. For CTMs that have a poorly resolved stratosphere or whose dynamics produce an unrealistic cross-tropopause ozone flux (as was the case for the GISS II fields), Synoz is the better candidate. For CTMs that do not suffer these shortcomings, Linoz is preferable because it produces a realistic and interactive stratospheric ozone field that allows for on-line calculation of ozone columns and photolysis/heating rates. Further, Linoz can also be used in GCMs, allowing feedback among ozone, heating rates, and the circulation. The next generation of Linoz will include important source gases for climate change in the 21st century. This would entail a chemistry that allows ozone to respond to evolving background concentrations of CH₄, stratospheric H₂O, N₂O, and stratospheric NO_y. A copy of the Linoz chemistry coefficients is available from the authors upon request.

Appendix: Photochemical Model

The photochemical box model of Prather [1992] and Prather and Jaffe [1990] is used to calculate the linearized ozone tables. While the basic model remains unchanged, there have been several improvements. The general chemistry set includes includes 101 kinetic reactions, 36 photolysis reactions, and 43 species (although not all of these are required for the tendency calculations, as discussed below). Reaction rate coefficients and absorption cross sections are adopted from DeMore *et al.* [1997]. Exceptions to the former include OH+NO₂ [Brown *et al.*, 1999a] and OH+HNO₃ [Brown *et al.*, 1999b].

The following seven heterogeneous reactions known to occur on and/or in sulfate aerosols have been added:



The rates are treated as pseudo-first order reactions in which the rate co-efficient is expressed in the form

$$k_i = \frac{\gamma_i}{4} c_i S, \quad (\text{A8})$$

where γ_i is the uptake coefficient (or reaction probability) for gas-phase species i , c_i is the thermal velocity of

<i>Set by Climatology or Tracer Correlations</i>			
O ₃	H ₂ O	CH ₄	CO
H ₂	NO _y	Cl _y	Br _y
<i>Calculated To Be in 24-Hour Steady State</i>			
O	O(¹ D)	HCHO	CH ₃ O ₂
CH ₃ OOH	OH	HO ₂	H
H ₂ O ₂	N	NO	NO ₂
NO ₃	N ₂ O ₅	HNO ₃	HONO
HNO ₄	HCl	Cl	ClO
Cl ₂	Cl ₂ O ₂	OCIO	HOCl
ClONO ₂	BrCl	HBr	Br
BrO	HOBr	BrONO ₂	

Figure A1. List of species and families used in the photochemical box model calculations of ozone tendency. Reactions involving the long-lived source gases, such as N₂O and the CFCs, are not included in the radical balance. Therefore, with the families NO_y, Cl_y and Br_y specified as here, these source gases do not directly impact the calculations.

species i , and S is the sulfate surface area density. Uptake coefficients for the first five reactions, (A1)–(A5), possess a strong temperature dependence [DeMore *et al.*, 1997; Hendricks *et al.*, 1999] and only become important at low temperatures. The last two, reactions (A6) and (A7), have a temperature independent uptake coefficient ($\gamma_{\text{N}_2\text{O}_5} = 0.1$; $\gamma_{\text{BrONO}_2} = 0.8$) [DeMore *et al.*, 1997]. A background sulfate surface-area density climatology (18 altitudes, 18 latitudes, 4 seasons) derived from SAGE II measurements [e.g., Thomason *et al.*, 1997] is used. Polar stratospheric clouds and ternary aerosols inside the polar vortex are not included.

For the calculations of ozone tendencies performed in this study, ozone, the families (NO_y, Cl_y, and Br_y), CO, and the hydrogen reservoirs (CH₄, H₂O, and H₂) are set by climatology and/or tracer correlations. With the families specified, long-lived source gases such as N₂O and CFCs are not included in the radical balances and thus do not directly impact these calculations (although there is an indirect impact because they are still used in tracer correlations). The remaining species are calculated to be in 24-hour steady state. All species and families used in these calculations are given in Figure A1, and details concerning their initialization can be found elsewhere [Avallone and Prather, 1997]. The box model is integrated for 30 days with the diurnal cycle fixed at mid-month. In the evaluation of the derivatives the second tendency calculation (based on a perturbed value of local ozone, temperature, or column ozone) is initialized using the same radical concentrations as the first.

Acknowledgments. UCI acknowledges the support of the atmospheric chemistry programs of NSF and NASA as well as the NASA Atmospheric Effects of Aviation Program. The authors thank two anonymous referees for their helpful comments.

References

- Appenzeller, C., J. R. Holton, and K. H. Rosenlof, Seasonal variations of mass transport across the tropopause, *J. Geophys. Res.*, **101**, 15,071–15,078, 1996.
- Avallone, L. A. and M. J. Prather, Tracer-tracer correlations: Three-dimensional model simulations and comparisons to observations, *J. Geophys. Res.*, **102**, 19,233–19,246, 1997.
- Brasseur, G. and S. Solomon, *Aeronomy of the Middle Atmosphere*, 441 pp., D. Reidel, Norwell, Mass., 1986.
- Brown, S. S., R. K. Talukdar, and A. R. Ravishankara, Rate constants for the reaction $\text{OH} + \text{NO}_2 + \text{M} \rightarrow \text{HNO}_3 + \text{M}$ under atmospheric conditions, *Chem. Phys. Lett.*, **299**, 277–284, 1999a.
- Brown, S. S., R. K. Talukdar, and A. R. Ravishankara, Reconsideration of the rate constant for the reaction of hydroxyl radicals with nitric acid, *J. Phys. Chem.*, **103**, 3,031–3,037, 1999b.
- Cariolle, D., and M. Déqué, Southern Hemisphere medium-scale waves and total ozone disturbances in a spectral general circulation model, *J. Geophys. Res.*, **91**, 10,825–10,846, 1986.
- Chipperfield, M. P., Multiannual simulations with a three-dimensional chemical transport model, *J. Geophys. Res.*, **104**, 1,781–1,805, 1999.
- Crutzen, P. J., M. G. Lawrence, and U. Poschl, On the background photochemistry of tropospheric ozone, *Tellus, Ser. A*, **51**, 123–146, 1999.
- de Grandpré, J., J. W. Sandilands, J. C. McConnell, S. R. Beagley, P. C. Croteau, and M. Y. Danilin, Canadian middle atmosphere model: Preliminary results from the chemical transport module, *Atmos. Ocean*, **35**, 385–431, 1997.
- DeMore, W. B., S. P. Sander, D. M. Golden, R. F. Hampson, M. J. Kurylo, C. J. Howard, A. R. Ravishankara, C. E. Kolb, and M. J. Molina, Chemical kinetics and photochemical data for use in stratospheric modeling, in Evaluation 12, *JPL Publ. 97-4*, Jet Propul. Lab., Pasadena, Calif., 1997.
- Douglass, A. R., R. B. Rood, S. R. Kawa, and D. J. Allen, A three-dimensional simulation of the evolution of the middle latitude winter ozone in the middle stratosphere, *J. Geophys. Res.*, **102**, 19,217–19,232, 1997.
- Fahey, D. W., et al., In situ observations of NO_y , O_3 , and the NO_y/O_3 ratio in the lower stratosphere, *Geophys. Res. Lett.*, **23**, 1,653–1,656, 1996.
- Hall, T. M., and M. J. Prather, Seasonal evolutions of N_2O , O_3 , and CO_2 : Three-dimensional simulations of stratospheric correlations, *J. Geophys. Res.*, **100**, 16,699–16,720, 1995.
- Hall, T. M., D. W. Waugh, K. A. Boering, R. A. Plumb, Evaluation of transport in stratospheric models, *J. Geophys. Res.*, **104**, 18,815–18,839, 1999.
- Hannegan, B., S. Olsen, M. Prather, X. Zhu, D. Rind, and J. Lerner, The dry stratosphere: A limit on cometary water influx, *Geophys. Res. Lett.*, **25**, 1,649–1,652, 1998.
- Hauglustaine, D. A., G. P. Brasseur, S. Walters, P. J. Rasch, J.-F. Müller, L. K. Emmons, and M. A. Carroll, MOZART, a global chemical transport model for ozone and related chemical tracers, 2, Model results and evaluation, *J. Geophys. Res.*, **103**, 28,291–28,335, 1998.
- Hendricks, J., E. Lippert, H. Petry, and A. Ebel, Heterogeneous reactions on and in sulfate aerosols: Implications for the chemistry of the midlatitude tropopause region, *J. Geophys. Res.*, **104**, 5,531–5,550, 1999.
- Intergovernmental Panel on Climate Change (IPCC), *Climate Change 1994: Radiative Forcing of Climate Change*, edited by J. T. Houghton, L. G. Meira Filho, J. Bruce, H. Lee, B. A. Callander, E. Haites, N. Harris, and K. Maskell, 339 pp., Cambridge Univ. Press, New York, 1995.
- Isaksen, I., and C. Jackman, Modeling the Chemical Composition of the Future Atmosphere, in *Aviation and the Global Atmosphere, IPCC Special Report*, edited by J. E. Penner, D. H. Lister, D. J. Griggs, D. J. Dokken, and M. McFarland, pp. 121–163, Cambridge Univ. Press, New York, 1999.
- Keim, E. R., et al., Measurements of the $\text{NO}_y\text{-N}_2\text{O}$ correlation in the lower stratosphere: Latitudinal and seasonal changes and model comparisons, *J. Geophys. Res.*, **102**, 13,193–13,212, 1997.
- Ko, M. K. W., N. D. Sza, and D. K. Weisenstein, Use of satellite data to constrain the model-calculated atmospheric lifetime for N_2O : Implications for other trace gases, *J. Geophys. Res.*, **96**, 7,547–7,552, 1991.
- Koch, D. and D. Rind, $^{10}\text{Be}/^{7}\text{Be}$ as a tracer of stratospheric transport, *J. Geophys. Res.*, **103**, 3,907–3,917, 1998.
- Logan, J. A., An analysis of ozonesonde data for the troposphere: Recommendations for testing 3-D models and development of a gridded climatology for tropospheric ozone, *J. Geophys. Res.*, **104**, 16,115–16,149, 1999a.
- Logan, J. A., An analysis of ozonesonde data for the lower stratosphere: Recommendations for testing models, *J. Geophys. Res.*, **104**, 16,151–16,170, 1999b.
- McPeters, R., Ozone profile comparisons, in *The Atmospheric Effects of Stratospheric Aircraft: Report of the 1992 Models and Measurements Workshop, NASA Ref. Publ. 1292*, edited by M. J. Prather and E. E. Remsburg, pp. D1–D37, 1993.
- Murphy, D. M. and D. W. Fahey, An estimate of the flux of stratospheric reactive nitrogen and ozone into the troposphere, *J. Geophys. Res.*, **99**, 5,325–5,332, 1994.
- Murphy, D. M., D. W. Fahey, M. H. Proffitt, S. C. Liu, K. R. Chan, C. S. Eubank, S. R. Kawa, and K. K. Kelly, Reactive nitrogen and its correlation with ozone in the lower stratosphere and upper troposphere, *J. Geophys. Res.*, **98**, 8,751–8,773, 1993.
- Nagatani, R. M., and J. E. Rosenfield, Temperature, net heating and circulation, in *The Atmospheric Effects of Stratospheric Aircraft: Report of the 1992 Models and Measurements Workshop, NASA Ref. Publ. 1292*, edited by M. J. Prather and E. E. Remsburg, pp. A1–A47, 1993.
- Phillips, N. A., The general circulation of the atmosphere: A numerical experiment, *Q. J. R. Meteorol. Soc.*, **14**, 184–185, 1956.
- Prather, M. J., Numerical advection by conservation of second-order moments, *J. Geophys. Res.*, **91**, 6,671–6,681, 1986.
- Prather, M. J., Catastrophic loss of stratospheric ozone in dense volcanic clouds, *J. Geophys. Res.*, **97**, 10,187–10,191, 1992.
- Prather, M. J., and A. H. Jaffe, Global impact of the antarctic ozone hole: Chemical propagation, *J. Geophys. Res.*, **95**, 3,473–3,492, 1990.
- Prather, M. J., M. McElroy, S. Wofsy, G. Russell, and D. Rind, Chemistry of the global troposphere: Fluorocarbons as tracers of air motion, *J. Geophys. Res.*, **92**, 6,578–6,613, 1987.
- Prather, M. J., M. M. Garcia, and R. Suozzo, Global impact of the Antarctic ozone hole: Dynamical dilution with a three-dimensional chemical transport model, *J. Geophys. Res.*, **95**, 3,449–3,471, 1990.
- Rind, D., R. Suozzo, N. K. Balachandran, A. Lacis, and G. Russell, The GISS global climate/middle atmosphere model, I, Model structure and climatology, *J. Atmos. Sci.*, **45**, 329–370, 1988.
- Rozañov, E. V., V. A. Zubov, M. E. Schlesinger, F. L. Yang, and N. G. Andronova, The UIUC three-dimensional

- stratospheric chemical transport model: Description and evaluation of the simulated source gases and ozone, *J. Geophys. Res.*, *104*, 11,755-11,781, 1999.
- Smagorinsky, J., S. Manabe, and J. L. Holloway, Numerical results from a nine-level general circulation model of the atmosphere, *Mon. Weather Rev.*, *93*, 727-768, 1965.
- Steil B., M. Dameris, C. Bruhl, P. J. Crutzen, V. Grewe, M. Ponater, and R. Sausen, Development of a chemistry module for GCMs: First results of a multiannual integration, *Ann. Geophys.*, *102*, 205-228, 1998.
- Sundet, J. K., Model studies with a 3-D global CTM using ECMWF data, Ph.D. thesis, Univ. of Oslo, 1997.
- Thomason, L. W., L. R. Poole, and T. Deshler, A global climatology of stratospheric aerosol surface area density deduced from Stratospheric Aerosol and Gas Experiment II measurements: 1984-1994, *J. Geophys. Res.*, *102*, 8,967-8,976, 1997.
- Wang, Y. H., J. A. Logan, and D. J. Jacob, Global simulation of tropospheric O₃-NO_x-hydrocarbon chemistry, 2, Model evaluation and global ozone budget, *J. Geophys. Res.*, *103*, 10,727-10,755, 1998.
- Wild, O., X. Zhu, and M. J. Prather, Fast-J: Accurate simulation of in- and below-cloud photolysis in global chemical models, *J. Atmos. Chem.*, in press, 2000.
- World Meteorological Organization (WMO), *Scientific Assessment of Ozone Depletion: 1998*, WMO Rep. No. 44, 732 pp., Global Ozone Res. and Monit. Proj., Geneva, 1999.
-
- B. Hannegan, Senate Energy and Natural Resources Committee, Dirksen Senate Office Building Room SD-308, Washington, DC 20510-6510.
- C. McLinden, S. Olsen, M. Prather, Department of Earth System Science, University of California at Irvine, Irvine, CA 92697-3100. (cmclinden@halo.ps.uci.edu.)
- J. Sundet, Department of Geophysics, University of Oslo, Box 1022, N-0315 Oslo, Norway.
- O. Wild, Frontier Research System for Global Change, Sumitomo Hamamatsu-cho Building, 4th Floor, 1-18-16 Hamamatsu-cho, Minato-ku, Tokyo 105-0013, Japan.

(Received December 16, 1999; revised February 14, 2000; accepted February 16, 2000.)